JGR Planets

RESEARCH ARTICLE
10.1029/2019JE006035

Magnetic Properties of Asteroid (162173) Ryugu

David Hercik[1], Hans-Ulrich Auster[1], Dragos Constantinescu[1,2], Jürgen Blum[1], Karl-Heinz Fornaçon[1], Masaki Fujimoto[3], Kathrin Gebauer[1], Jan-Thimo Grundmann[4], Carsten Güttler[5], Olaf Hillenmaier[6], Tra-Mi Ho[4], Andreas Hördt[1], Christian Krause[7], Ekkehard Kührt[8], Laurence Lorda[9], Ayako Matsuoka[3], Uwe Motschmann[8,10], Aurélie Moussi-Soffys[9], Ingo Richter[1], Kaname Sasaki[4], Frank Scholten[8], Bernd Stoll[1], Benjamin P. Weiss[11], Friederike Wolff[12], and Karl-Heinz Glassmeier[1,5]

[1]Institut für Geophysik und extraterrestrische Physik, Technische Universität Braunschweig, Braunschweig, Germany, [2]Institute for Space Sciences, Magurele, Romania, [3]Institute of Space and Astronautical Science, JAXA, Kanagawa, Japan, [4]Institute of Space Systems, DLR, Bremen, Germany, [5]Max-Planck-Institut für Sonnensystemforschung, Göttingen, Germany, [6]Magson GmbH, Berlin, Germany, [7]Microgravity User Support Center, DLR, Cologne, Germany, [8]Institute of Planetary Research, DLR, Berlin, Germany, [9]Centre National d'Etudes Spatiales, Toulouse, France, [10]Institut für Theoretische Physik, Technische Universität Braunschweig, Brunswick, Germany, [11]Department of Earth, Atmospheric, and Planetary Sciences, Massachusetts Institute of Technology, Cambridge, MA, USA, [12]Institute of System Dynamics and Control, DLR, Wessling, Germany

Key Points:
- The study reveals magnetic measurements of a C-type asteroid Ryugu during landing of MASCOT, the Hayabusa2 lander
- Observations show no global magnetic moment consistent with Ryugu being a rubblepile asteroid
- Local magnetization down to centimeter scales is also not detected, indicating nonmagnetic material or magnetization on lower scales

Correspondence to:
D. Hercik,
d.hercik@tu-bs.de

Citation:
Hercik D., Auster, H.-U., Constantinescu, D., Blum, J., Fornaçon, K.-H., Fujimoto, M., et al. (2020). Magnetic properties of asteroid (162173) Ryugu. *Journal of Geophysical Research: Planets*, *125*, e2019JE006035. https://doi.org/10.1029/2019JE006035

Received 23 MAY 2019
Accepted 22 DEC 2019
Accepted article online 2 JAN 2020

Author Contributions
Formal Analysis: Frank Scholten
Visualization: Frank Scholten
Writing - review & editing: Frank Scholten

©2020. The Authors.
This is an open access article under the terms of the Creative Commons Attribution-NonCommercial License, which permits use, distribution and reproduction in any medium, provided the original work is properly cited and is not used for commercial purposes.

Abstract Observations of the magnetization state of asteroids indicate diverse properties. Values between 1.9×10^{-6} Am^2/kg (Eros) and 10^{-2} Am^2/kg (Braille) have been reported. A more detailed understanding of asteroidal magnetic properties allows far-reaching conclusions of the magnetization mechanism as well as the strength of the magnetic field of the solar system regions the asteroid formed in. The Hayabusa2 mission with its lander Mobile Asteroid Surface Scout is equipped with a magnetometer experiment, MasMag. MasMag is a state-of-the-art three-axis fluxgate magnetometer, successfully operated also on Philae, the Rosetta mission lander. MasMag has enabled, after Eros for the second time ever, to determine the magnetic field of an asteroid during descent and on-surface operations. The new observations show that Ryugu, a low-albedo C-type asteroid, has no detectable global magnetization, and any local magnetization is either small ($< 10^{-6}$ Am^2/kg) or on very small (subcentimeter) scales. This implies, for example, that energetic solar wind particles could reach and alter the surface unimpeded by strong asteroidal magnetic fields, such as minimagnetospheres in case of the Moon.

Plain Language Summary Magnetic measurements in space near and on solar system bodies such as asteroids can provide important information about their formation history and their material properties. Hayabusa2, a Japanese mission, visited asteroid Ryugu, a type of asteroid (carbon rich) not visited before. Ryugu is a rubble pile, that is, an agglomeration of rocks and boulders. It is not expected to have any global magnetic field, but it can be magnetized on smaller scales (boulders or pebbles). Hayabusa2 carried therefore a small lander called Mobile Asteroid Surface Scout equipped also with an instrument for magnetic field measurement (magnetometer). In this study, we present observations from the magnetometer that were collected during Mobile Asteroid Surface Scout's descent and landing on the surface of Ryugu. The magnetic measurements show that Ryugu is not magnetized on boulder (greater than centimeter) scales. This gives us indication on its origin and evolution. In particular, it shows that Ryugu and the bodies it was created from did not possess any magnetic field generation mechanism and that they were not created in an environment with strong background magnetic field. The results are important inputs for theories about the solar system evolution that work with magnetic field as one of the drivers for dust accretion and planetary formation.

1. Introduction

The Mobile Asteroid Surface Scout (MASCOT) (Ho et al., 2017) is a small lander on the Hayabusa2 mission (Watanabe et al., 2017) of the Japan Aerospace Exploration Agency investigating the near-Earth asteroid 162173 Ryugu (provisional designation 1999 JU_3) (Wada et al., 2018). Hayabusa2's main mission goal is to bring material samples from the asteroid's surface back to Earth. During the remote operations, the

spacecraft was monitoring the surface of Ryugu, using visible, thermal, and near-infrared imagers to characterize the body morphologically and thermally. The MASCOT lander provided in situ observations of the surface morphology, surface temperature, and magnetic field. The MASCOT payload comprises a camera (CAM) (Jaumann et al., 2017), a radiometer (MARA) (Grott et al., 2017), an infrared spectrometer (MicrOmega) (Bibring et al., 2017), and a magnetometer (MasMag) (Herčík et al., 2017).

MASCOT successfully separated from Hayabusa2 on 3 October 2018 around 2 a.m. UTC and landed after a few bounces (at least four bounces visible significantly changing the MASCOT's trajectory together with a nondetermined number of microbounces) several minutes later on the surface of Ryugu. MasMag continuously measured for about 12.5 hr after separation. The observations cover the descent and bouncing phase as well as on-surface day and night measurements. In the present study, we will focus on the magnetization characteristics of Ryugu and its material. Ryugu is categorized as a Cb-type asteroid (Watanabe et al., 2019). The Hayabusa2 observations show very low albedo (geometric albedo ∼4.5 and reflectance ∼1.88% at 0.55 μm) and three main types of boulders of the surface (Sugita et al., 2019). The material from the spectral measurements resembles CV, CM, or CI type of carbonaceous chondrite meteorites. The closest match from Hayabusa2 near-infrared observations is with heated Ivuna (CI1) meteorite (Kitazato et al., 2019). MASCOT camera, on the other hand, revealed morphology features, like abundance of calcium-aluminum-rich inclusions, comparable to CV or CM meteorites (Jaumann et al., 2019).

There are extensive studies of magnetic properties of carbonaceous chondrites (Banerjee & Hargraves, 1972; Carporzen et al., 2011; Emmerton et al., 2011; Fu et al., 2014). The results show a range of natural remanent magnetization (NRM) typically in the order of 10^{-5} to 10^{-3} Am^2/kg for chondrules and also for the matrix and the bulk material. The higher limit could be probably influenced either by weathering (in case of falls) in the Earth's magnetic field or by magnets used by some collectors. Several hypotheses were formulated to explain the meteoritic magnetization: either in the preaccretional phase by solar nebula magnetic field (Fu & Weiss, 2012; Nübold & Glassmeier, 2000) or in the postaccretional phase by internal dynamo of the parent body (Weiss et al., 2010).

To support meteoritic paleomagnetic measurements, in situ observations at the asteroids are extremely valuable, because they provide geologic context and measurements over much larger spatial scales. However, such measurements are sparse. Preceding MASCOT, there was only one direct magnetic measurement from the surface of Eros (S-type) by a magnetometer on the NEAR spacecraft during its final crash landing (Acuña et al., 2002). Other magnetic observations were conducted by the Philae lander on a comet 67P/Churyumov-Gerasimenko (Heinisch et al., 2018). Both measurements found no detectable signal related to the surface fields and provided therefore only an upper limit on the material specific magnetic moment. The specific magnetic moment means in this study a total bulk magnetic moment of a given sample per kilogram. The specific magnetic moment, as a normalized value, is used to enable comparison to other studies dealing with meteorite's or asteroid's magnetization, although, as we will show later, it is not a always straightforward comparison.

Other measurements come from asteroid flybys: Gaspra's (Kivelson et al., 1993) and Braille's (Richter et al., 2001) magnetic signatures during flybys led to an estimate of the specific magnetic moment of $\sim 10^{-2}$ Am^2/kg. In case of Gaspra, the asteroidal magnetic field origin was questioned by Blanco-Cano (2003), who argued that the measured signature could be also a solar wind feature. In case of Braille, the signature at the closest approach was within solar wind variability (approximately nanotesla) and therefore also not conclusive. No signature was measured during Rosetta Šteins (Auster et al., 2010) and Lutetia (Richter et al., 2012) flybys. Hence, there is no fully conclusive evidence for bulk magnetization of the visited asteroids. The overview of the measurements in space is given in Table 1. The table gives estimated values (in the last row, orders of magnitude only) for specific magnetic moment of the visited small bodies. In case there was no magnetic signature detected during flyby or landing, the value (noted with "<") gives only an upper limit of the specific magnetic moment. The value of the measured field in these cases (also noted with "<") indicates the overall measurement accuracy under given environmental conditions that is mainly depending on the variability of the background magnetic field. This value was used for the moment upper limit estimation, as the measurement accuracy gives the maximum signal, that can be hidden within the data. The accuracy of the instrumentation itself is usually well below 0.1 nT. None of the visited asteroids was a C-type asteroid such as Ryugu. It is also to be noted that the best candidate for a bulk magnetism, a metal M-type asteroid, remains still to be encountered by a magnetometer equipped mission.

Table 1
An Overview of Magnetic Observations of Small Bodies

Body	Gaspra	Braille	Šteins	Lutetia	Eros	67P
Mean radius (km)	7	0.8	3	49	9	~4
Density (kg/m^3)	4,000	3,900	3,200	3,400	2,650	533
CA (km)	1,600	28	799	3,120	landing	landing
Measured field (nT)	draping[a]	2	<1	<1	<5	<0.9
Spec. magnetic moment (Am^2/kg)	~10^{-2}	~10^{-2}	<10^{-3}	<10^{-7}	<10^{-6}	<10^{-5}

Note. Specific magnetic moment given either directly in the relevant paper or derived from therein provided magnetic moment. The references for the respective properties are for *Gaspra* (Kivelson et al., 1993), *Braille* (Richter et al., 2001), *Šteins* (Auster et al., 2010), *Lutetia* (Coradini et al., 2011; Richter et al., 2012), *Eros* (Acuña et al., 2002; McCoy et al., 2001), and *67P* (Heinisch et al., 2018). The magnetization values for simplicity show orders of magnitude only. CA = closest approach.
[a]Deformation of magnetic field lines in front of an obstacle for a solar wind flow, in this case no increase in magnetic field measured.

Direct comparison of the in situ measurements with meteoritic studies is not straightforward. Even if the material property is specific magnetic moment, that is, the strength of the magnetization normalized to mass, the values might not be comparable in a straightforward manner. The scale/dimension of the measured sample still matters. The reason for that is the scale of homogeneity of the magnetic domains. If all the domains in a sample are aligned unidirectionally, then bulk magnetic moment is high and, also, the derived specific moment will be high and will correspond to the one on single domain scale. On the contrary, when the domains are randomly oriented, the total bulk field produced will be more or less canceled out and the estimated specific moment much smaller than the one of a single domain. This effect is already mentioned by Wasilewski et al. (2002) when comparing meteoritic data with magnetic observations on Eros. The authors point out that even the same meteoritic material, investigated within their study, shows inverse dependence of the specific magnetic moment on the sample size. Therefore, we are discussing our observations below with respect to the assumed magnetic heterogeneity scale.

The MASCOT magnetometer measurements provide consequently magnetization constraints that are highly complementary to meteorite studies. Also, they will provide invaluable geologic context to future paleomagnetic measurements of samples that may be returned to Earth by Hayabusa2 enabling a cross-scale magnetization comparative study. One should, however, note that the measurements cannot be generalized to the entire C-type group of asteroids, as Ryugu is a rubble pile probably recreated after catastrophic disruption consisting of different types of material (boulders) (Sugita et al., 2019). The authors, however, indicate that the impact had apparently no significant influence on the thermal history of Ryugu's material itself. The homogeneity of the material in terms of weak 7-μm absoption band points more toward an internal heating mechanism in the parental body. Therefore, high temperatures erasing the NRM are probably not to be expected in the history of Ryugu.

2. Measurements

2.1. Instrument

The MASCOT magnetometer instrument was developed at the Institut für Geophysik und extraterrestrische Physik, Technische Universität Braunschweig in Germany. It is based on heritage from previous space missions, such as THEMIS (Auster et al., 2008), Rosetta (Auster et al., 2007), or Venus Express (Zhang et al., 2007). MasMag is a fluxgate magnetometer measuring three components of the magnetic field at 10 Hz with a dynamic range of ±12,000 nT, digital resolution of 2 pT, and internal sensor noise <15 pT/$\sqrt{\text{Hz}}$ at 1 Hz.

The instrument was calibrated on ground in the Magnetsrode facility of the TU-Braunschweig. The sensor head is not boom-mounted but is located in the corner of the MASCOT lander body. This accommodation leads to a high level of magnetic AC and DC interference coming from the spacecraft flight system itself. Therefore, an extensive campaign was carried out in order to characterize the interference from the MASCOT flight system and its subunits. The campaign description as well as other detailed information about the instrument can be found in Herčík et al. (2017).

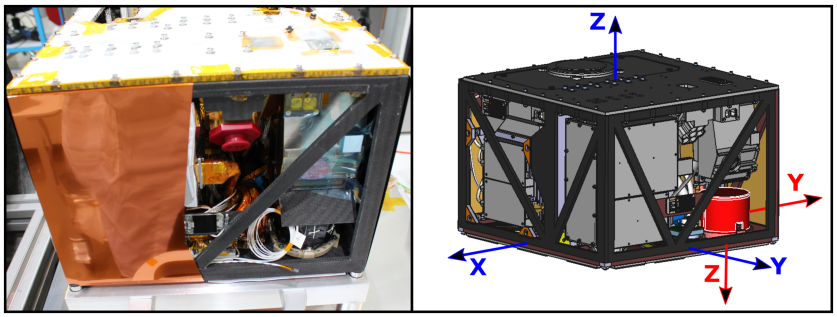

Figure 1. (left) Photo of MASCOT lander during the ground measurement campaign. The MasMag instrument is accommodated in the lower right corner. (right) CAD model of MASCOT with the magnetometer sensor head highlighted in red. The blue axes show the coordinate system of the lander, and the red axes show the coordinate system of the magnetometer. The MasMag *x* axis goes along the negative *y* axis of the lander.

Figure 1 shows the MASCOT lander with MasMag accommodation in the lower right corner under the camera instrument and indication of lander and magnetometer coordinates.

2.2. Objectives

The objectives for the MASCOT magnetometer are to observe any global or local magnetic fields coming from the asteroid itself. In order to determine the specific magnetic moment of the asteroid, continuous observation during descent is needed. Magnetic properties related to local features (boulders or craters) can be determined during the bouncing and hopping over the surface. The size of MASCOT and the proximity of MasMag to the surface of the asteroid enables determination on uniform magnetization down to the ~10-cm scale. This is an important piece of information bridging the scale from flyby measurements and results from laboratory small-scale investigations of meteorites. Another important step will be the magnetic characterization of the samples that Hayabusa2 will return to Earth.

2.3. Operations

After separation from the Hayabusa2 spacecraft, MASCOT dropped to the surface of Ryugu from a height of about 40 m. After about 6 min, MASCOT hit a large boulder (~3 m in size), rebounded and started bouncing on the surface, finally coming to rest ~20 min after separation. MASCOT's rebound on the large boulder provides an exclusive opportunity to study magnetically a larger structure on the surface. The ground path of the descent trajectory over reconstructed terrain is shown in Figure 2. The full reconstruction of the MASCOT trajectory can be found in Scholten et al. (2019).

The MasMag instrument was switched on about 3 hr before the separation and stayed on continuously for almost 12.5 hr, when it was switched off by a telecommand to save power. The magnetometer was then switched on again twice during the rest of the mission for a short time (several minutes) check. The first long continuous measurement provides a unique data set including the descent magnetic field profile and on-surface measurements during the asteroid day and night.

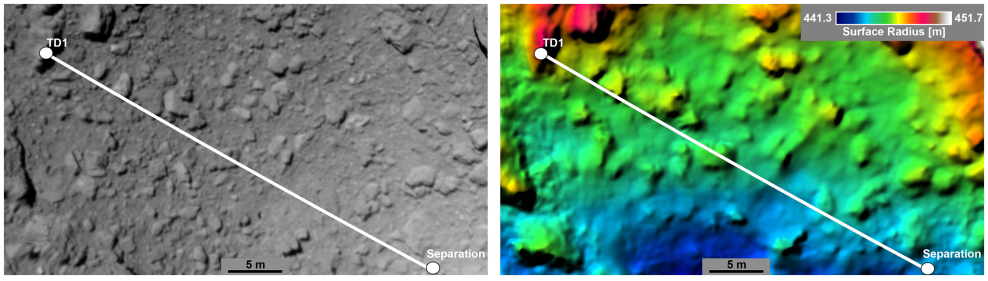

Figure 2. The MASCOT landing site area as characterized by images from the Optical Navigation Camera (ONC) onboard Hayabusa2 (Preusker et al., 2019; Scholten et al., 2019). The left panel shows a rectified ONC image map. The right panel shows an ONC image-based digital terrain model of the same area in color-coded hill-shaded relief representation. The white line displays the ground path of the descent trajectory of MASCOT from its separation until its first contact point TD1 on the surface of Ryugu.

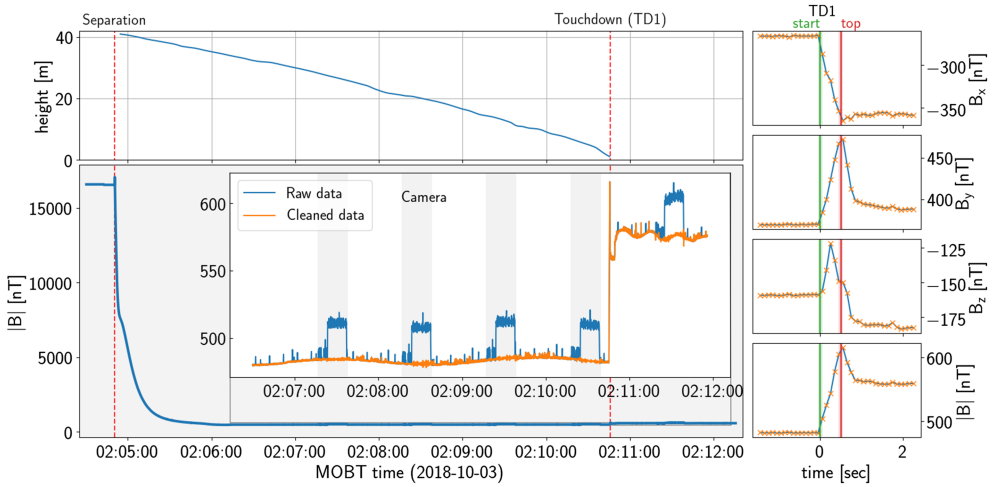

Figure 3. The left-side panel shows at the bottom the magnetic field magnitude measured by MasMag during the separation of MASCOT from Hayabusa2 and during its descent toward Ryugu with the first contact with the surface. The inset figure, zoomed in the vertical axis, shows the observed field (blue curve) with the interference of the MASCOT camera signatures, while taking images (gray shaded), and with the interference cleaned (orange curve). The upper left panel gives the height over the local surface as derived from visibilities of MASCOT and its shadow within Hayabusa2 ONC images; details of the full trajectory can be found in Scholten et al. (2019). The right panels show detailed magnetic field signature (the three components and the magnitude) of the first touchdown (TD1) event.

Figure 3 shows a single component of the magnetic field as observed by MasMag during MASCOT's descent toward the Ryugu surface. The separation of MASCOT from the Hayabusa2 spacecraft is clearly visible in the magnetic field data and was one of the direct confirmations of the success of the separation procedure. The inset figure, zoomed in the vertical axis, shows the observed data (in blue), where interference from the camera instrument is clearly visible. The interference, caused by the camera, is a step-like interference caused by the increased current consumption of the camera instrument while taking an image as well as during the image processing afterward. Fortunately, during the interesting phase, camera settings were the same. The interference profile is highly deterministic and could be removed. We removed the interference by creating camera signature with a superposed epoch analysis using 10 signatures and building the average, that was used for cleaning the data of the camera interference by subtracting the average signature from the time series for each camera image occurrence.

The orange curve shows the data cleaned of this interference. The cleaned data still contain a DC offset generated by the MASCOT system. On top of the offset, oscillations are visible, caused by the MASCOT's rotation during the free flight within the quasi-static external field, where the amplitude of the oscillations is determined by the external field magnitude. The first contact with the surface, marked as “Touchdown(TD1)” in the figure, is associated with an event in which the magnetic field increases over 0.5 s by ~135 nT in magnitude. The change in the magnetic field is an abrupt event. The profile of the field increase does not follow a $1/r^3$ increase, which would be expected in case the source of the field would be located on the surface of the asteroid. The field drops from the peak value in about ~0.4 s by 50 nT, leaving the MASCOT offset on a ~85 nT higher level than before the touchdown. This behavior indicates that the internal MASCOT offset has changed during the contact with the surface. Therefore, we conclude that the field change is not related to any surface magnetization but most likely to the change within the MASCOT body itself. The cause could be a movement of some subsystem part (e.g., harness) caused by deceleration and after rebound acceleration of MASCOT.

3. Data Processing

The data acquired during the asteroid measurements need to be carefully processed and cleaned. The raw data contain lots of interference and disturbances from the MASCOT subsystems. The cleaning procedure and data analysis were done in the following steps.

1. *Major interference removal*. This is a semiautomatic procedure based on the on-ground cleanliness campaign. Several types of interference coming from other subunits with clear and deterministic profiles are

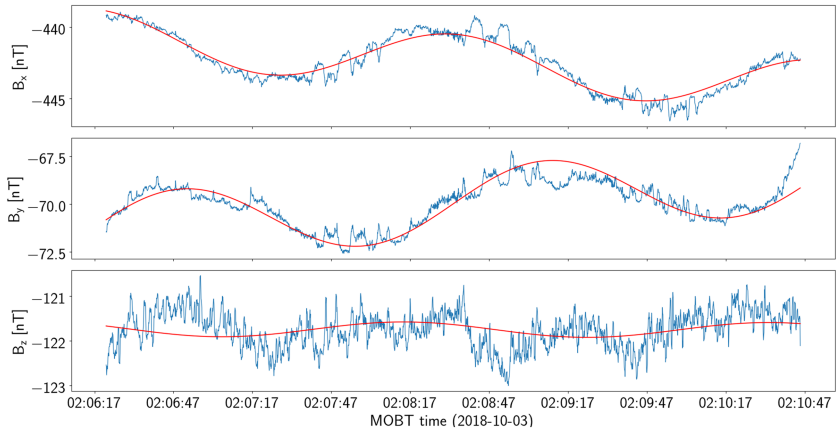

Figure 4. MasMag data in the variance coordinate system (see main text for explanation) with least squares fit. The panels show magnetic field components with maximum, intermediate, and minimum variance (from top to bottom). The red curve shows the fit of the rotation taking into account constant background field and linear offset. The linear trend in the offset is visible in the first two panels.

removed. For the removal of the signature, a superposed epoch method is used. Several (tens) events are averaged into a single generic profile characteristic for a specific event type. Then this general profile is removed from every single occurrence of such event. An example can be seen in Figure 3, in the inset axis showing a signature of the camera taking an image. This profile is deterministic and sufficiently stable to be safely removed from the data. Another example is a periodic signal appearing as a single sharp peak with a constant period. There are several such signals identified in the data, which are related to onboard computer activities (e.g., housekeeping readouts). This signal can be also removed from the time series easily by setting the peak value (single data point) to the average of neighboring data points.

2. *Removal of disturbances*. There are still lots of smaller disturbances remaining in the data after the first pass of cleaning. These kinds of interferences have no clear signature in the time series. However, it appears that the disturbances have a predominant direction, as they are probably generated by the electrical current changes flowing in the common electronic box. Therefore, we conducted the following analysis. First, we filtered the data with a high-pass filter to separate the disturbances from the low-frequency oscillations. The high-pass filtering was implemented by first smoothing the original data with a running average window of 10 data points (1 s). The average (low-pass-filtered) signal was then subtracted from the original data, leaving higher-frequency part of the data, for the interference extraction.
   The high-pass-filtered data were used for finding the maximum variance direction by applying maximum variance analysis (Sonnerup & Scheible, 1998). Building the covariance matrix from the three magnetic field components and computing eigenvectors and eigenvalues, we got the direction (indicated by the eigenvector with the maximum eigenvalue) in which the variance of the field is maximal. Then we transformed the original magnetic field data from the instrument coordinates into the variance system. By the variance system, we mean the coordinate system with vector basis defined by the eigenvectors coming from the maximum variance analysis of the high-pass-filtered data. The first component is the one corresponding to the eigenvector with the highest eigenvalue, that is, having the maximum variance. The hodogram and the time series of the transformed data show that the main high-frequency disturbances are well separated in the first component. The other two components remain clear of these types of disturbances. The first component in the variance system was hence smoothed by a running average with a boxcar window with 10 data points length. The cleaned data in the variance system were in the end rotated back into the original MasMag coordinate system. The data with the disturbances removed were further used for the analysis described below.
3. *Offset determination*. The MASCOT spacecraft is not magnetically clean and causes also a magnetic DC offset at the magnetometer sensor position. The magnetic cleanliness characterization on ground with results and comparison to in-flight characteristics is given in Herčík et al. (2017). The offset caused by the separate MASCOT lander can be seen in Figure 4 approximately as the average value, where the data are shown in a coordinate system with minimum variance on the z axis. Fortunately, during the descent, MASCOT was spinning, which provides us a possibility to determine the MASCOT offsets. Because DC

offsets are fixed in the MASCOT frame, during the MASCOT's rotation MasMag sees a fixed offset field with a superposed rotating external contribution. This is clearly visible in Figure 4 on the top two panels. The external field (the interplanetary magnetic field and any asteroid contribution) is quasi-homogeneous in the inertial frame. As MASCOT rotates within this field, it observes a sinusoidal signal around the zero level in the spin plane. We used again the variance analysis, this time on the data cleaned from the main sources of disturbance as discussed in the previous step. The purpose is to find the rotation axis, which should be roughly aligned with the minimum variance direction. As the main part of the MASCOT's disturbance is removed, the variance in the signal is caused by the rotating (from MASCOT's perspective) external magnetic field. Therefore, the maximum and intermediate variance direction gives us the spin plane. The converted data into the variance system are used to find the rotation period, amplitude, and offset using a least squares fit. For the model parameters, we assume a constant background field, linearly changing DC offsets, rotation axis, rotation period, and its initial phase. The assumption about constant magnetic field is used solely for the fit purposes and does not influence the data postprocessing. On the contrary, the offset gained from the fit is removed from the data before despinning. The assumption of linearly changing offset is reasonable, as the temperature of MASCOT changed during the descent and offset is in general temperature dependent. The offset change is not caused by the magnetometer itself, as its temperature stability is in the order of 20 pT/K and the temperature change of the sensor itself during the descent was about 1 °C. However, some MASCOT units saw temperature change of about 10 °C, which could cause change in magnetic properties. Unfortunately, there were no preflight magnetic temperature calibrations of the whole MASCOT, so this is only assumption. Nevertheless, thanks to the rotation, a change in offset can be distinguished from a change in the background field. A linear change in offset would translate into a linear trend in the data displayed in Figure 4; a change in background magnetic field would result in changing the amplitude of the sinusoidal oscillations. Therefore, with the fit and despin procedure, we are not removing any important information about the change in background field. It is to be noted that the linear trend in the spin-plane components, which we model as linear offset drift, can be also possibly explained by a MASCOT's precession motion with much larger period than the rotation. The two possibilities are hard to distinguish as the analyzed time period is too short compared to assumed precession. However, as this is only geometrical effect, it would also not change the resulting external field estimate. The fit profile is shown by the red curve in Figure 4. The offset changes during the analyzed period by ∼2 nT. The fit parameters used for the despinning of the data yield the rotation period of 138.9 s. The rotation axis of the MASCOT lander coming from the fit is $a = (-0.71, -0.62, 0.34)$ in MasMag internal coordinates and $a = (0.62, 0.71, -0.34)$ in MASCOT lander coordinate system. This converted to spherical coordinates means azimuth $\phi = 49°$ and elevation $\theta = -20°$.

4. *Data despin*. The fitted parameters were used for despinning the data and for the offset removal. The linear offset, coming from the previous fit, was removed from all three components. It should be noted that the offset that was removed is completely recovered from the fit only in the rotational plane. The fit cannot distinguish between the DC value of the external magnetic field component in the rotation axis and an internal offset along the axis. However, any constant contribution of the external magnetic field for the whole time period is not important for the further analysis. The data without offset were then despun; that is, each vector was rotated around the rotation axis by an angle corresponding to reversed rotation as given by the fit. The resulting data are in an inertial system that can be related to the asteroid body fixed frame, once the attitude of the MASCOT during the descent is known. For our analysis, however, the orientation of the system relative to Ryugu is not important. The result represents the best effort cleaned and calibrated data from the period just before (100 ms) the first contact with the surface. The final data are displayed in Figure 5. Here, the three components of the magnetic field are shown in the upper three panels, and the magnetic field magnitude is displayed in the bottom panel. Although the data still probably contain some interference from the MASCOT flight system, the variation mainly reflects the background magnetic field. The data set starts when MASCOT is at a height of about 32 m above the surface (from the motion analysis by the MASCOT's flight dynamics team and the image analysis of the MASCOT's camera team) and the last data point is just before the first contact with the surface. The variation during this interval is in the order of 1 nT, and there is no increase visible in the magnitude with the decreasing distance to the surface. The magnitude of the observed external magnetic field is for the whole period between 1 and 3 nT, which is consistent with a typical interplanetary magnetic field at the distance of 1.24 AU (heliocentric distance of Ryugu at the time of MASCOT operation).

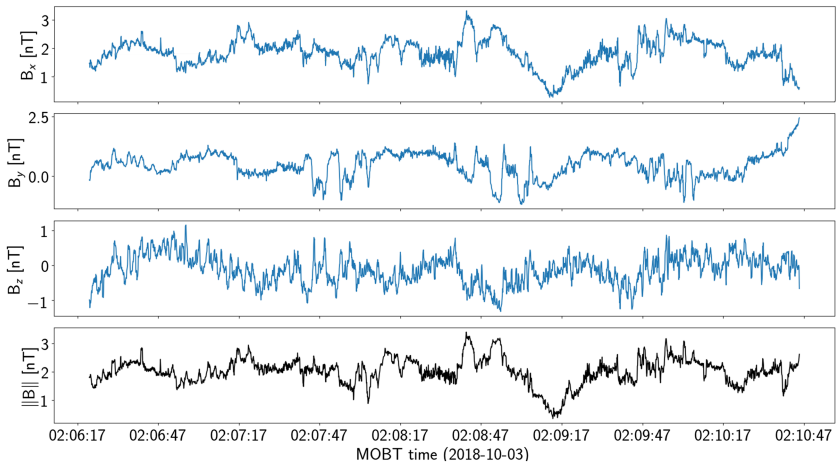

Figure 5. Best effort cleaned and calibrated data in an inertial frame. The top three panels show the field components, and the last panel shows the field magnitude. The magnitude reveals only background variations coming from the solar wind and possibly some remaining disturbances from the MASCOT. However, there is no gradual change indicating any surface located sources. The data correspond to MASCOT being at a distance of ∼32 m above the surface (beginning of the shown data) until 0.1 s before hitting the surface (equals to distance of ∼2 cm above the surface).

4. Results

There is no visible change in the magnetic field as MASCOT is approaching Ryugu up to the first contact with the surface (CP1). The first contact of MASCOT with Ryugu was observed by the Hayabusa2 ONC camera. Therefore, we know that MASCOT hit a boulder about ∼3 m in diameter (see also Figure 2). Based on the observations and assumptions on material density, we estimate the upper limit for Ryugu's magnetization.

In order to calculate the upper limit estimate, we will follow the procedure described and justified in detail in Auster et al. (2015). There, we have shown that a magnetic field profile above the surface can be approximated by a single dipole in the second Gaussian orientation (field measured above the dipole center in the direction perpendicular to the dipole direction). This approximation assumes the surface to consist of magnetic domains, where each single magnetic domain is represented by a single magnetic dipole located in the center of the domain. This representation reflects the fact that the magnetic domain itself is homogeneously magnetized in its volume. Mutually, these domain dipoles can be randomly oriented, that is, the material is magnetically heterogeneous above the magnetic domain dimension scale. For the purpose of the study, we will name this magnetic domain dimension scale as the "magnetization scale," that is, the dimension, on which is the material homogeneously magnetized. It is an unknown parameter that needs to be determined by other means.

As discussed in detail in the supporting information in Auster et al. (2015), a volume of material, represented by a set of magnetic domains as described above, can be characterized, in terms of magnetic field profile above the surface, by a single domain dipole. If the magnetic domain has a dimension of d (= magnetization scale), then the dipole is located in depth $d/2$ below the surface, is oriented parallel to the surface, and has the same magnitude as the other magnetic domain dipoles. This can be explained by the fact that in a large set, randomly oriented dipoles statistically cancel out each other's contribution and the magnetic field is detectable only close to the single domains on their size scale.

The magnetic field in the magnetic equator plane (second Gaussian orientation) of a single dipole with a magnetic moment M along a radial distance r can be expressed as

$$B = C\frac{M}{r^3}, \tag{1}$$

where C is a constant ($\mu_0/4\pi$ for SI units).

We further assume that the magnetic domain is a sphere that is represented by a single magnetic dipole moment $M = m\rho V[\mathrm{Am}^2]$, where m is specific magnetic moment (normalized to mass, $[\mathrm{Am}^2/\mathrm{kg}]$),

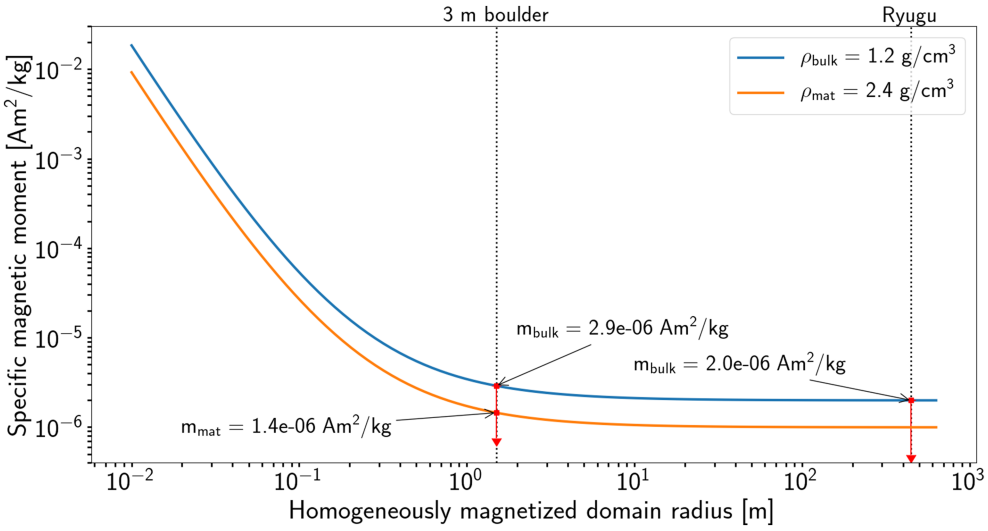

Figure 6. Estimate of the specific magnetic moment of Ryugu's material in dependence on the radius of the homogeneously magnetized domains (r_b) ~ magnetization scale.

$V = \frac{4}{3}\pi r_b^3$ is the volume of one magnetic domain with radius r_b, and ρ is the material density. This gives

$$B = C\frac{m\rho\frac{4}{3}\pi r_b^3}{(h + r_b)^3}, \tag{2}$$

where h is the height above the surface of the single modeled magnetic domain.

We now apply this general approach for our analysis in case of Ryugu. From the variations of the background field displayed in Figure 5, we estimate the maximum magnetic field contribution from Ryugu's material to the measured fields to be less than 1 nT (B_0). Hence, we can express the specific magnetic moment m as dependent on h and r_b as

$$m(B, h, r_b) = \frac{B}{C\rho\frac{4}{3}\pi}\left(\frac{h}{r_b} + 1\right)^3. \tag{3}$$

Setting a limit for $B = B_0$ (the measured field at the height h above surface), we can compute the specific magnetic moment as a function of height h and homogeneously magnetized sphere radius r_b.

For the computation, we use the following assumptions for the situation, when MASCOT touches the Ryugu surface for the first time:

$B_0 = 1$ nT	approximately the variation of the measured magnetic field before the contact
$h = 0.2$ m	estimated distance of the magnetometer from the surface
$\rho_{bulk} = 1.2$ g/cm^3	bulk density of Ryugu
$\rho_{mat} = 2.4$ g/cm^3	assuming 50% porosity.

The density of the material is needed for the calculation of the specific magnetic moment. We can either take into account the bulk density as measured by Hayabusa2 (Watanabe et al., 2019) or assume 50% porosity yielding the density of the material reaching values that are close to carbonaceous chondrites densities. This value is also in a range of porosities (between 22% and 55%) derived from MARA instrument measurements of thermal inertia and thermal conductivity (Grott et al., 2019).

The resulting estimate on the upper limit of the specific magnetic moment in dependence on the magnetization scale (the size of homogeneously magnetized domains) is shown in Figure 6. The magnetization scale is a measure of homogeneity of the magnetization direction; above this scale the magnetized material domains are nonunidirectionally oriented. In bulk material with dimensions larger than the mentioned scale, the net magnetic field would near zero as statistically the random dipoles cancel out each other's contribution. Therefore, it is expected to observe significant magnetization only when measuring on the scales similar to

the homogeneous magnetization scale. Figure 6 shows specific moment estimate computed from equation (3) for two density values, orange for assumed material density of 2.4 g/cm^3 and blue for the asteroid's bulk density of 1.2 g/cm^3.

5. Conclusions

Apparently, the magnetization state of the Ryugu's surface material cannot be unequivocally determined from the MASCOT observations. We can only set an upper limit for the magnetization that moreover depends on the magnetic heterogeneity scale as demonstrated in Figure 6. MASCOT at the first contact hit a 3-m boulder. If we assume the boulder to be homogeneously magnetized on its dimensions scale, the upper limit for the specific magnetic moment would be 2.9×10^{-6} Am^2/kg, assuming a bulk density ρ_{bulk} of 1,200 kg/cm^3 and 1.4×10^{-6} Am^2/kg, assuming 50% macroporosity with a material density ρ_{mat} of 2,400 kg/cm^3. The real magnetization can be, however, higher in case the magnetization heterogeneity is on smaller scales.

The inner parts of carbonaceous chondrite meteorites show typically NRM values between 10^{-5} and 10^{-4} Am^2/kg when measuring several bulk samples. A detailed study of millimeter-sized Allende samples (Fu et al., 2014) showed uniform magnetization ($\sim 10^{-5}$ Am^2/kg) of the matrix and a nonuniform magnetization of the chondrules. The magnetic heterogeneity is on less than a millimeter scale. The net bulk moment of the matrix could be caused by a past dynamo in the parent body. If the matrix has a net uniform magnetization and the chondrules do not, then the chondrules may have gained or changed their magnetization state in the postdynamo era either by chemical remanent magnetization or by thermoremanent magnetization. The authors also exclude the preaccretional magnetization of the chondrules based on the heterogeneity of the magnetization across the single chondrules.

In case of Ryugu, there is no observable net field above the measurement accuracy at a distance ~20 to 10 cm from the surface material, indicating that the matrix of the surface material is not unidirectionally magnetized on decimeter scales exceeding magnetization values of $\sim 10^{-5}$ Am^2/kg. We cannot conclude from the measurement on the paleomagnetic intensities or with certainty exclude the possibility of a weak dynamo on the parent body of Ryugu. However, the lack of signal supports the hypothesis that the parent body of Ryugu possessed no dynamo and any magnetization of the material is rather nonunidirectional on less than centimeter scales. In that case, one explanation of the randomness of the magnetization could be preaccretional magnetization of the grains. The lack of magnetization on greater than centimeter scales limits the role of the preaccretional nebular magnetic field as an accretional mechanism. To conclude on that, however, we need to wait for Hayabusa2 to return back to Earth with the samples of the surface material from Ryugu. Paleomagnetic investigation on the return samples would therefore be of high value and could shed more light on the subject. Putting together the MasMag results and sample analysis would give us a cross-scale information about Ryugu.

Acknowledgments
The lead investigator group at the Technische Universität Braunschweig is financially supported by the Deutsches Zentrum für Luft- und Raumfahrt and the Bundesministerium für Wirtschaft und Energie under Contract 50OW1501. The MasMag team would like to acknowledge extensive support and help during integration and testing from the DLR MASCOT system team in Bremen lead by Tra-Mi Ho and MASCOT operation preparation and control before and during the landing from the DLR team in Köln lead by Christian Krause. The analysis was supported by CNES flight dynamics team and DLR Berlin camera team providing the estimated MASCOT trajectory. B. Weiss thanks the NASA Emerging Worlds program (Grant NNX15AH72G) for support. The data used for the study are available on the Harvard Dataverse (under https://doi.org/10.7910/DVN/ULEQVA). The fully calibrated and cleaned data from the whole mission will be available additionally on NASA PDS archive after the data acceptance review process during the year 2020.

References

Acuña, M. H., Anderson, B. J., Russell, C. T., Wasilewski, P., Kletetschka, G., Zanetti, L., & Omidi, N. (2002). NEAR magnetic field observations at 433 Eros: First measurements from the surface of an asteroid. *Icarus*, *155*(1), 220–228. https://doi.org/10.1006/icar.2001.6772

Auster, H.-U., Apathy, I., Berghofer, G., Fornacon, K.-H., Remizov, A., Carr, C., et al. (2015). The nonmagnetic nucleus of comet 67P/Churyumov-Gerasimenko. *Science*, *349*(6247), aaa5102. https://doi.org/10/f7kdh4

Auster, H.-U., Apathy, I., Berghofer, G., Remizov, A., Roll, R., Fornacon, K. H., et al. (2007). ROMAP: Rosetta magnetometer and plasma monitor. *Space Science Reviews*, *128*(1-4), 221–240. https://doi.org/10.1007/s11214-006-9033-x

Auster, H.-U., Glassmeier, K. H., Magnes, W., Aydogar, O., Baumjohann, W., Constantinescu, D., et al. (2008). The THEMIS Fluxgate Magnetometer. *Space Science Reviews*, *141*(1-4), 235–264. https://doi.org/10.1007/s11214-008-9365-9

Auster, H.-U., Richter, I., Glassmeier, K. H., Berghofer, G., Carr, C. M., & Motschmann, U. (2010). Magnetic field investigations during ROSETTA's 2867 Šteins flyby. *Planetary and Space Science*, *58*(9), 1124–1128. https://doi.org/10.1016/j.pss.2010.01.006

Banerjee, S. K., & Hargraves, R. B. (1972). Natural remanent magnetizations of carbonaceous chondrites and the magnetic field in the early solar system. *Earth and Planetary Science Letters*, *17*(1), 110–119. https://doi.org/10.1016/0012-821X(72)90265-8

Bibring, J.-P., Hamm, V., Langevin, Y., Pilorget, C., Arondel, A., Bouzit, M., et al. (2017). The MicrOmega investigation onboard Hayabusa2. *Space Science Reviews*, *208*(1-4), 401–412. https://doi.org/10.1007/s11214-017-0335-y

Blanco-Cano, X. (2003). Hybrid simulations of solar wind interaction with magnetized asteroids: Comparison with Galileo observations near Gaspra and Ida. *Journal of Geophysical Research*, *108*(A5), 1216. https://doi.org/10.1029/2002JA009618

Carporzen, L., Weiss, B. P., Elkins-Tanton, L. T., Shuster, D. L., Ebel, D., & Gattacceca, J. (2011). Magnetic evidence for a partially differentiated carbonaceous chondrite parent body. *Proceedings of the National Academy of Sciences*, *108*(16), 6386–6389. https://doi.org/10.1073/pnas.1017165108

Coradini, A., Capaccioni, F., Erard, S., Arnold, G., De Sanctis, M. C., Filacchione, G., et al. (2011). The surface composition and temperature of asteroid 21 Lutetia as observed by Rosetta/VIRTIS. *Science*, *334*(6055), 492–494. https://doi.org/10.1126/science.1204062

Emmerton, S., Muxworthy, A. R., Hezel, D. C., & Bland, P. A. (2011). Magnetic characteristics of CV chondrules with paleointensity implications. *Journal of Geophysical Research*, *116*, E12007. https://doi.org/10.1029/2011JE003856

Fu, R. R., Lima, E. A., & Weiss, B. P. (2014). No nebular magnetization in the Allende CV carbonaceous chondrite. *Earth and Planetary Science Letters*, *404*, 54–66. https://doi.org/10.1016/j.epsl.2014.07.014

Fu, R. R., & Weiss, B. P. (2012). Detrital remanent magnetization in the solar nebula: Accretional remanent magnetization. *Journal of Geophysical Research*, *117*, E02003. https://doi.org/10.1029/2011JE003925

Grott, M., Knollenberg, J., Borgs, B., Hänschke, F., Kessler, E., Helbert, J., et al. (2017). The MASCOT radiometer MARA for the Hayabusa 2 mission. *Space Science Reviews*, *208*(1-4), 413–431. https://doi.org/10.1007/s11214-016-0272-1

Grott, M., Knollenberg, J., Hamm, M., Ogawa, K., Jaumann, R., Otto, K. A., et al. (2019). Low thermal conductivity boulder with high porosity identified on C-type asteroid (162173) Ryugu. *Nature Astronomy*, *3*(11), 971–976. https://doi.org/10/ggdmmq

Heinisch, P., Auster, H.-U., Richter, I., & Glassmeier, K.-H. (2018). Revisiting the magnetization of comet 67P/Churyumov-Gerasimenko. *Astronomy & Astrophysics*, *630*, 5–9. https://doi.org/10.1051/0004-6361/201834278

Herčík, D., Auster, H.-U., Blum, J., Fornaçon, K.-H., Fujimoto, M., Gebauer, K., et al. (2017). The MASCOT magnetometer. *Space Science Reviews*, *208*(1-4), 433–449. https://doi.org/10.1007/s11214-016-0236-5

Ho, T.-M., Baturkin, V., Grimm, C., Grundmann, J. T., Hobbie, C., Ksenik, E., et al. (2017). MASCOT—The Mobile Asteroid Surface Scout Onboard the Hayabusa2 Mission. *Space Science Reviews*, *208*(1-4), 339–374. https://doi.org/10.1007/s11214-016-0251-6

Jaumann, R., Schmitz, N., Ho, T.-M., Schröder, S. E., Otto, K. A., Stephan, K., et al. (2019). Images from the surface of asteroid Ryugu show rocks similar to carbonaceous chondrite meteorites. *Science*, *365*(6455), 817–820. https://doi.org/10/gf7tp6

Jaumann, R., Schmitz, N., Koncz, A., Michaelis, H., Schroeder, S. E., Mottola, S., et al. (2017). The camera of the MASCOT asteroid lander on board Hayabusa 2. *Space Science Reviews*, *208*(1-4), 375–400. https://doi.org/10.1007/s11214-016-0263-2

Kitazato, K., Milliken, R. E., Iwata, T., Abe, M., Ohtake, M., Matsuura, S., et al. (2019). The surface composition of asteroid 162173 Ryugu from Hayabusa2 near-infrared spectroscopy. *Science*, *364*, eaav7432. https://doi.org/10/gfw8bh

Kivelson, M. G., Bargatze, L. F., Khurana, K. K., Southwood, D. J., Walker, R. J., & Coleman, P. J. (1993). Magnetic field signatures near Galileo's closest approach to Gaspra. *Science*, *261*, 331–334.

McCoy, T. J., Burbine, T. H., Mcfadden, L. A., Starr, R. D., Gaffey, M. J., Nittler, L. R., et al. (2001). The composition of 433 Eros: A mineralogical-chemical synthesis. *Meteoritics & Planetary Science*, *36*(12), 1661–1672. https://doi.org/10.1111/j.1945-5100.2001.tb01855.x

Nübold, H., & Glassmeier, K.-H. (2000). Accretional remanence of magnetized dust in the solar nebula. *Icarus*, *144*(1), 149–159. https://doi.org/10.1006/icar.1999.6273

Preusker, F., Scholten, F., Elgner, S., Matz, K.-D., Kameda, S., Roatsch, T., et al. (2019). The MASCOT landing area on Asteroid (162173) Ryugu: Stereo-photogrammetric analysis using images of the ONC onboard the Hayabusa2 spacecraft. *Astronomy & Astrophysics*, *632*, L4.

Richter, I., Auster, H. U., Glassmeier, K. H., Koenders, C., Carr, C. M., Motschmann, U., et al. (2012). Magnetic field measurements during the ROSETTA flyby at asteroid (21)Lutetia. *Planetary and Space Science*, *66*(1), 155–164. https://doi.org/10.1016/j.pss.2011.08.009

Richter, I., Brinza, D. E., Cassel, M., Glassmeier, K.-H., Kuhnke, F., Musmann, G., et al. (2001). First direct magnetic field measurements of an asteroidal magnetic field: DS1 at Braille. *Geophysical Research Letters*, *28*(10), 1913–1916. https://doi.org/10.1029/2000GL012679

Scholten, F., Preusker, F., Elgner, S., Matz, K.-D., Jaumann, R., Biele, J., et al. (2019). The descent and bouncing path of the Hayabusa2 lander MASCOT at asteroid (162173) Ryugu. *Astronomy & Astrophysics*, *632*, L3. https://doi.org/10.1051/0004-6361/201936757

Sonnerup, B. U. Ö., & Scheible, M. (1998). Minimum and maximum variance analysis. *ISSI Scientific Reports Series*, *1*, 185–220.

Sugita, S., Honda, R., Morota, T., Kameda, S., Sawada, H., Tatsumi, E., et al. (2019). The geomorphology, color, and thermal properties of Ryugu: Implications for parent-body processes. *Science*, *364*, eaaw0422. https://doi.org/10/gfw8bk

Wada, K., Grott, M., Michel, P., Walsh, K. J., Barucci, A. M., Biele, J., et al. (2018). Asteroid Ryugu before the Hayabusa2 encounter. *Progress in Earth and Planetary Science*, *5*(1), 82. https://doi.org/10.1186/s40645-018-0237-y

Wasilewski, P., Acuña, M. H., & Kletetschka, G. (2002). 443 Eros: Problems with the meteorite magnetism record in attempting an asteroid match. *Meteoritics & Planetary Science*, *37*(7), 937–950. https://doi.org/10.1111/j.1945-5100.2002.tb00868.x

Watanabe, S., Hirabayashi, M., Hirata, N., Hirata, N., Noguchi, R., Shimaki, Y., et al. (2019). Hayabusa2 arrives at the carbonaceous asteroid 162173 Ryugu-A spinning top-shaped rubble pile. *Science*, *364*, eaav8032. https://doi.org/10/gfw8bj

Watanabe, S., Tsuda, Y., Yoshikawa, M., Tanaka, S., Saiki, T., & Nakazawa, S. (2017). Hayabusa2 Mission overview. *Space Science Reviews*, *208*(1-4), 3–16. https://doi.org/10.1007/s11214-017-0377-1

Weiss, B. P., Gattacceca, J., Stanley, S., Rochette, P., & Christensen, U. R. (2010). Paleomagnetic records of meteorites and early planetesimal differentiation. *Space Science Reviews*, *152*(1-4), 341–390. https://doi.org/10.1007/s11214-009-9580-z

Zhang, T. L., Berghofer, G., Magnes, W., Delva, M., Baumjohann, W., Biernat, H., et al. (2007). MAG: The Fluxgate Magnetometer of Venus Express. *ESA Special Publication*, *SP 1295*, 10.